Film Formation of Latex Blends with Bimodal Particle Size Distributions: Consideration of Particle Deformability and Continuity of the Dispersed Phase

A. Tzitzinou and J. L. Keddie*

Department of Physics, School of Physics and Chemistry, University of Surrey, Guildford, Surrey GU2 5XH, U.K.

J. M. Geurts, A. C. I. A. Peters, and R. Satguru

Avecia b.v., PO Box 123, Waalwijk 5140 AC, The Netherlands

Received August 12, 1999; Revised Manuscript Received December 15, 1999

ABSTRACT: Latex dispersions having a well-controlled, bimodal particle size distribution are gaining attention because they potentially enable control of the dispersion rheology, the film formation characteristics, and the final film properties. Here we study the film formation of dispersions with a bimodal particle size distribution (large:small size ratio of ca. 6:1) and with varying concentrations of the two particle sizes. We also compare the film formation of blends containing only deformable (i.e., "soft") particles with blends containing both soft and nondeformable (i.e., "hard") particles. We use ellipsometry as a noninvasive tool for studying film morphology as film formation proceeds. We interpret our ellipsometry data using a physical model of the morphology based on atomic force microscopy observation. Electron microscopy of film cross sections provides information about the bulk morphology. We measure void content and surface roughness in blend films as a function of the concentration of large particles for three series of blends based on soft particles only and on the two combinations of hard and soft particles. When large and small soft particles are blended above a small particle concentration of ca. 16.5 wt % (corresponding to a number ratio of small:large of 43:1), the void concentration in freshly prepared films reaches a low value. This concentration approximately corresponds to the critical volume fraction (V_c) of small particles required to obtain a continuous phase of small particles surrounding the large particles. Below this value, there are not enough small particles to create a continuous phase, so more interparticle voids are present in the film. Surface roughness and void volume concentration in blends of large−soft and small−hard particles also reach a minimum at V_c. At higher concentrations of small−hard particles, void concentration increases because the continuous phase is non-film-forming. Finally, when large−hard particles are blended with small−soft particles, film formation is hindered by the clustering of the large particles and the subsequent creation of voids. In this case, film formation at concentrations of small particles below about ca. 45 wt % cannot be achieved. A coherent film cannot be obtained at small particle concentrations nearer to or below V_c.

1. Introduction

Within the past several years, the use of latex blends has gained increased attention in the literature,[1] which reflects an even greater amount of study in industry. Of particular interest are (1) blends of large and small particles, (2) blends of film-forming and non-film-forming (i.e., "hard" and "soft") particles, and (3) blends with both various sizes and hardnesses. Research by Winnik and Feng[2] has shown that hard/soft latex blends can be used to achieve films that produce lower levels of volatile organic compound (VOC) (compared to formulations containing a coalescent that evaporates during film formation) and thus are less damaging to human health and the environment. Eckersley and Helmer[3] have demonstrated that careful control of large/small size ratio and hard/soft concentration ratio can produce composite films with desired film formation characteristics and also with enhanced blocking resistance and mechanical properties. Latex dispersions with controlled particle size distributions have been devised so as to increase the solids content and thereby minimize solvent usage while gaining additional control of viscosity.[4] As the viscosity of a colloidal dispersion depends on the particle size,[5] the control of particle size distribution has a pronounced effect on the rheology of latex dispersions.

Underlying the development of latex blend films are several implicit or explicit aims in blending large and small latex particles. One aim might be for a single small particle to fill each interstitial void produced by the close-packing of the large particles. The size ratio of large:small particle diameters will determine the type of interstitial void that the small particles will be able to fill. For instance, if the ratio is 4.45:1, then a small particle will be able to fill a tetrahedral void formed by the face-centered packing of four large particles in analogy with the zinc blende crystal structure.[6] In this scenario, the number ratio of large:small particles should be 1:1. Several years ago, Bartlett et al.[7] obtained colloidal crystals with the composition AB_2 and AB_{13} from careful control of large (A) to small (B) particles. In principle, therefore, it is technically feasible to form a latex film from a colloidal crystal. Such a film would presumably be highly dense and void-free as a result of efficient particle packing. In most real latex blends, however, higher concentrations are used, and there is a certain amount of polydispersity of sizes in the parent dispersions. Thus, in practice, films derived from latex colloidal crystals are not a realistic aim. Moreover, as

* To whom correspondence should be addressed. E-mail: j.keddie@surrey.ac.uk.

10.1021/ma991372z CCC: $19.00
Published on Web 03/10/2000

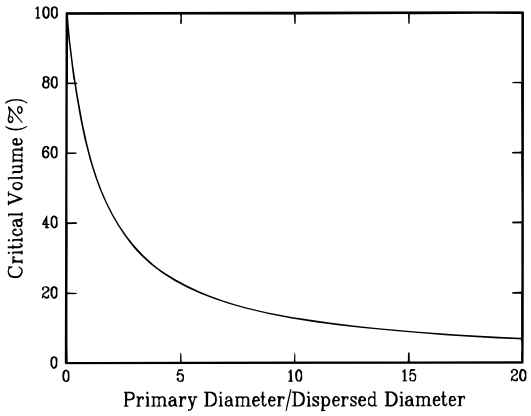

Figure 1. Critical volume percent above which the dispersed (i.e., small particle) phase is continuous around primary (i.e., large) particles for various size ratios of primary to dispersed particles. The calculations are based on the equations of Kusy[12] assuming that the critical concentration is defined a continuous, dispersed, hexagonally packed phase around each primary particle. At a large:small size ratio of 6:1 (as used here), the critical volume concentration, V_c, which is the *minimum* concentration of small particles required for continuity, is about 18%.

Geurts et al.[8] have pointed out, particle packing can be affected by particle stability and the clustering of particles of the same size. In a hard/soft blend, the clustering of hard particles has been shown to create air voids[9] that are filled exceedingly slowly by the soft phase. Such air voids cause light scattering and thereby lead to film opacity.[10] In a similar vein, it has been known for several decades that void fractions as low as 0.0384 can be obtained in blends of hard particles if the particle size ratios are carefully controlled and if five or more particle sizes are used.[11] Such a strategy would require very tight control of particle sizes and is likewise not realistic in most applications.

An alternative aim of bimodal blends has been proposed by Eckersley and Helmer.[3] They have made use of the concepts of phase continuity (developed by Kusy[12]) to suggest that optimal particle packing is achieved when the smaller particles form a continuous phase around the larger particles. The minimum volume fraction of small particles that is required to achieve a continuous phase is defined as the critical volume fraction, V_c. The value of V_c has been calculated as a function of the size ratio of large:small particles.[12] In Figure 1 we plot the critical volume percent of the dispersed phase (i.e., small particles), which is required to achieve a continuous network of these particles around the primary phase (i.e., large particles), in the terminology used in refs 3 and 12. (Note that V_c should not be confused with the percolation threshold, which is the critical fraction to achieve *connectivity* of the phase but not to form a *continuous* phase.) In the work presented here, the ratio of the primary to the dispersed phase diameters is about 6:1. Figure 1 shows that for this size ratio, V_c of the dispersed phase, according to the continuity calculation, is ca. 0.18. Physically, this means that when the void volume fraction of small particles is 0.18, there will be just enough small particles to surround the large particles and to fill the void space between them, thereby resulting in an efficient particle packing. One might expect that efficient particle packing will correlate with optimal film formation and low permeability in latex films. In this work, we explore film formation characteristics above, below, and near the V_c of 0.18.

Experimentally, the work of Peters et al.[13] supports Kusy's concepts of phase continuity. They studied a blend of large and small latex particles having a size ratio of 6:1. The V_c for this size ratio is predicted to be about 20 vol % of small particles. At concentrations of small particles below this critical value, there is evidence for interparticle voids as indicated by permeability measurements. In a related study, Guerts et al.[8] considered how the minimum film-formation temperature (MFT) varied with the concentration of small particles in a blend of particles with a size ratio of 10.4:1. V_c for this size ratio is estimated to be about 12 vol %. A latex blend with a volume fraction of small particles *above* this critical value was found to have a low MFT value, similar to the MFT of the latex consisting of only small particles. This result is consistent with what is expected for a continuous phase of small particles. Blends with concentrations of small particles *below* this critical value had a relatively high MFT, similar to the MFT of a latex consisting of only large particles. In this latter case, the small particles are not continuous and therefore cannot eliminate the voids associated with the large particles, so that the MFT is not made lower.

These and other previous results[9,10] indicate that the second scenario (based on concepts of phase continuity) is a more desirable and practical aim. In this present work, we monitor interstitial void concentration for blends with different concentrations of large and small particles. We investigate how the void volume concentration of films varies with the concentrations of large and small soft particles, and we determine which concentration is ideal in order to achieve improved packing properties, as reflected in the minimization of the concentration of air voids. We compare the film formation of soft blends to those that contain both hard and soft particles with the same size ratios.

2. Experimental Materials and Procedure

2.1 Latex Dispersions. The latex dispersions used here were prepared by semibatch emulsion polymerization using sodium dodecyl sulfate (SDS) to achieve stability and ammonium persulfate as the initiating salt. The latex composition is based on a copolymer of butyl acrylate, methyl methacrylate, and methyl acrylic acid. Further details on the synthesis are given elsewhere.[13] Table 1 provides some characteristics of the four parent latex dispersions used in making the latex blends. Two parameters of particular relevance to this study are the particle size and the glass transition temperature. The polymers with a glass transition temperature (T_g) of 20 °C are referred to here as "soft" as a means of achieving conciseness with clarity. We refer to the high T_g particles as "hard". The refractive indices of the acrylic polymers (also listed in the table) were determined from ellipsometry measurements of thin films (>100 nm thick) prepared by spin-casting latex copolymer solutions in toluene onto silicon substrates.

Bimodal blends were prepared by mixing different fractions (by weight) of the large and small particle size dispersions. Specifically, we prepared three series of blends.

Series 1: large−soft and small−soft (LgSf/SmSf).

Series 2: large−soft and small−hard (LgSf/SmHd).

Series 3: large−hard and small−soft (LgHd/SmSf).

We will refer to the particle types using the abbreviations shown in Table 1 and in parentheses above. The blends were stirred continuously for at least 15 h to ensure a uniform dispersion. Table 2 lists the concentrations of large particles in the blends according to both weight fraction and number ratio.

Table 1. Latex Characteristics of Dispersions Having Monomodal Particle Size Distributions

description (abbreviation)	mean particle[a] size (nm)	polydispersity	solids content (wt %)	glass transition temp (°C)	refractive index at 500 nm
small and soft (Sm/Sf)	50.0	1.18	40.5	20	1.4886
large and soft (Lg/Sf)	297.2	1.26	52.0	20	1.4886
small and hard (Sm/Hd)	50.0	1.15	50.5	80	1.4970
large and hard (Lg/Hd)	286.0	1.16	41.0	80	1.4970

[a] Particle sizes were measured by photon correlation spectroscopy (Otsuka ELS800).

Table 2. Number Ratio of Small-to-Large Particles for Various Blends

wt % large particles used	N_{small}/N_{large}	wt % large particles used	N_{small}/N_{large}
100	0	56	150
99	2	24	681
92	19	12	1533
83.5	43	0	∞

2.2 Film Formation. Samples used for analysis by ellipsometry, AFM, and SEM were prepared by casting the dispersions onto glossy black card substrates under identical conditions. The card was attached to a rigid substrate to prevent bending. Typically 0.5 mL of dispersion was spread over a substrate area of 6 cm × 6 cm using a casting bar. Film formation took place in still air under the ambient conditions of the laboratory. Temperature and relative humidity were measured during each experiment. The final latex film thickness achieved by this method was approximately 80 μm.

2.3. Film Characterization. 2.3.1. Atomic Force Microscopy (AFM) and Scanning Electron Microscopy (SEM). Images providing information about latex film morphology and viscoelasticity were obtained with an atomic force microscope (Digital Instruments, Nanoscope III) in the tapping mode. At least three different regions of each surface were imaged to verify reproducibility and to ensure that a truly representative image was obtained. The results were also reproduced for up to three different samples prepared separately.

Although atomic force microscopy is a relatively new technique,[14] its use is already well-established in the study of latex film formation, as was recently discussed.[1] Use of tapping mode AFM is particularly suitable for soft latex surfaces[15,16] that are liable to be disturbed by mechanical forces imposed by the AFM tip in the contact mode. Tapping mode provides two types of images: the height and the phase image. The height image (usually shown on the left-hand side) provides topographical characterization of the surface, and the phase image (on the right-hand side) provides some indication of the viscoelastic properties. Phase images are known to be more sensitive to particle interfaces, which is particularly useful in the case of the small (50 nm) particles studied here. Small particles are clearly revealed in the phase images, even in cases where they cannot be seen in topographical (height) images.

In some cases, images of film cross sections were obtained with scanning electron microscopy (SEM) to complement images of the film surface obtained with AFM. SEM analysis was performed 4 days after the film preparation. The films were immersed in liquid nitrogen after peeling from the substrate. They were then fractured in a direction normal to the surface while still at a low temperature. The fractured surfaces were sputter-coated with a thin film of gold to make the surface conducting. The cross sections were analyzed at room temperature in the electron microscope (Hitachi S-3200N). A low accelerating voltage of 15 kV and a low beam current of ≈70 μA were used to minimize the amount of damage during the experiment.

2.3.2. Ellipsometry. Ellipsometry was performed using a Woollam variable angle spectroscopic ellipsometer (VASE), which incorporates a rotating-analyzer configuration.[17] Ellipsometry is sensitive to the refractive index profile of the material under investigation. In turn, the refractive index is a function of material density, composition and morphology.[18] Ellipsometry provides a noninvasive means of measuring surface roughness and the concentration of nanovoids in latex films. The use of ellipsometry in probing latex film formation has been reported previously.[9,19,20]

Ellipsometry determines the change of the state of polarization of light upon reflection from a surface or interface. In an experiment, two parameters (known as Ψ and Δ) are measured. Prior to reflection, the polarization of light is characterized by the amplitude ratio of the components in the plane of reflection (p-component) and perpendicular to this plane (s-component), designated as A_p/A_s. The difference in phase between the two components (designated as δ_p-δ_s) is zero in the case of the linearly-polarized light used here. Upon reflection, both the amplitude ratio and the phase difference usually change. Δ is defined as this change in the phase after the reflection

$$\Delta = (\delta_p{}^r - \delta_s{}^r) - (\delta_p{}^i - \delta_s{}^i) = (\delta_p{}^r - \delta_s{}^r) \quad (1)$$

where r represents the reflected light and i, the incident light. The parameter Ψ is the ratio of the amplitude ratio before and after the reflection:

$$\tan \psi = \frac{A_p^r/A_s^r}{A_p^i/A_s^i} \quad (2)$$

The ellipsometric angles Ψ and Δ are related to the Fresnel reflection coefficients through the equation of ellipticity:

$$\rho = \frac{R_p}{R_s} = \tan \Psi \exp(i\Delta) \quad (3)$$

where R_p and R_s are the Fresnel reflection coefficients for the p- and s-planes, respectively, and ρ is the ellipticity. The Fresnel reflection coefficients are directly related to the complex refractive indices of the two media at a planar interface.

Two types of ellipsometry analysis were performed: dynamic scans and variable-angle scans. In a dynamic scan, we determined Ψ and Δ at a fixed wavelength and angle-of-incidence, ϕ_o, at time intervals of 2 s. during the course of latex film formation, starting with a wet dispersion and finishing with a polymer film. The dynamic scans were initiated with a time delay of approximately 5 min after the deposition of the dispersion onto the substrate. Typically scans were obtained with light in the visible region (500, 600, or 700 nm) at an angle-of-incidence of 56°, corresponding to the Brewster angle of a dry film where greatest sensitivity is obtained. All the dynamic scans were performed either at room temperature (22−25 °C) or on a temperature-controlled stage at a temperature of 24 °C, in cases where the room temperature was lower than 22 °C. The relative humidity of the room was 45−55%.

In a variable-angle scan, which takes approximately 2 min to perform, we determined ψ and Δ as a function of ϕ_o from a film 1 h after casting on the substrate. Variable-angle scans provide sufficient data to determine with certainty the void concentration and surface roughness of a latex film, as will be explained later.

2.3.3. Spectrophotometry. A double-beam UV−visible spectrophotometer (Camspec M350) was used to measure optical transmission of films prepared from various blends over

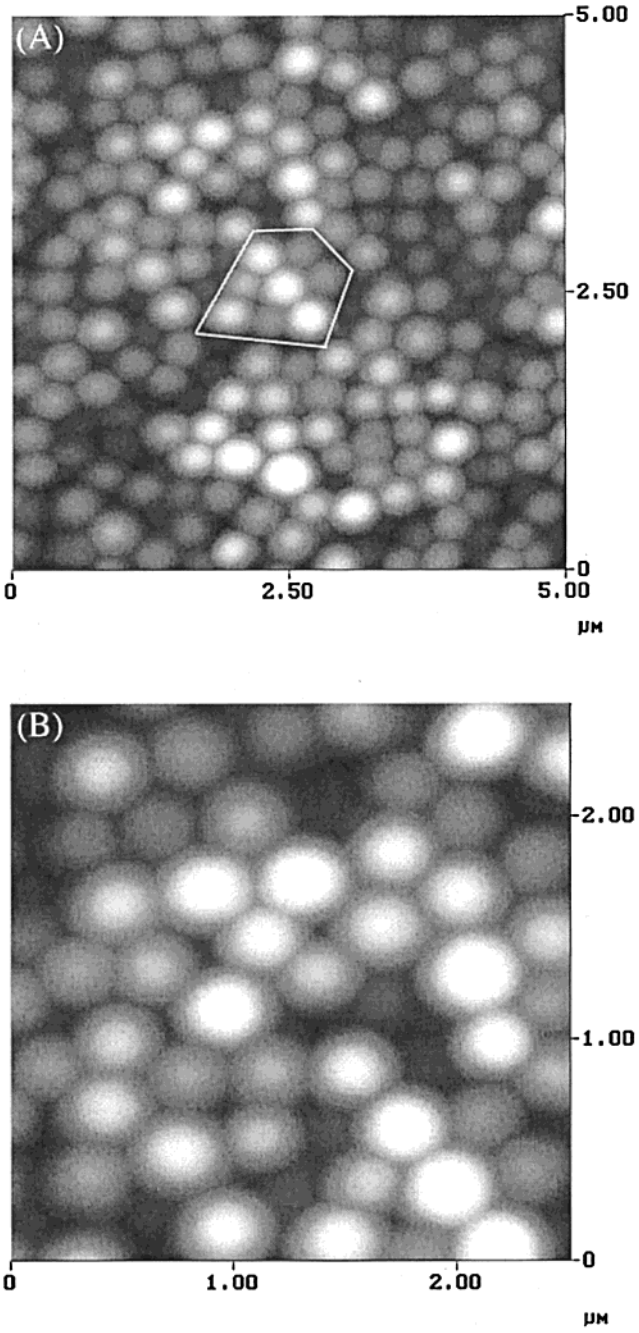

Figure 2. AFM topographical images of the polymer−air interface of a film prepared from LgSf latex particles, showing a large (A) area (5 μm × 5 μm) and small (B) area (2.5 μm × 2.5 μm). In part A, regions of more densely packed particles can be seen, such as indicated by the white lines. In part B, interparticle voids can be seen as well as larger voids where there are defects in particle packing.

the wavelength range from 500 to 800 nm. Samples prepared for spectrophotometry were cast on clean glass slides at room temperature (22−25 °C) using a consistent casting method in order to achieve similar final thicknesses (≈ 80 μm). The samples were then left to dry and film-form in air for an hour at a relative humidity of ca. 45% before analysis at room temperature.

3. Results and Discussion

3.1 Microscopy. AFM reveals the surface morphology and particle packing of films prepared from the various blends of large and small particles. Figure 2 shows an AFM scan of the polymer−air interface of a latex film cast from a monomodal dispersion of LgSf particles. As can be seen, particles at the polymer/air interface tend to cluster together to form close-packed domains. These domains are separated from each other by disruptions in the packing in which particles appear to be missing. This type of structure gives rise to relatively high average surface roughness. Additionally, at points of contact between particles, there is deformation from a spherical shape. Even so, particles retain their identity (at least at the film surface), and there is no particle coalescence. Interparticle voids are readily seen, even though visually the bulk film is continuous and glossy.

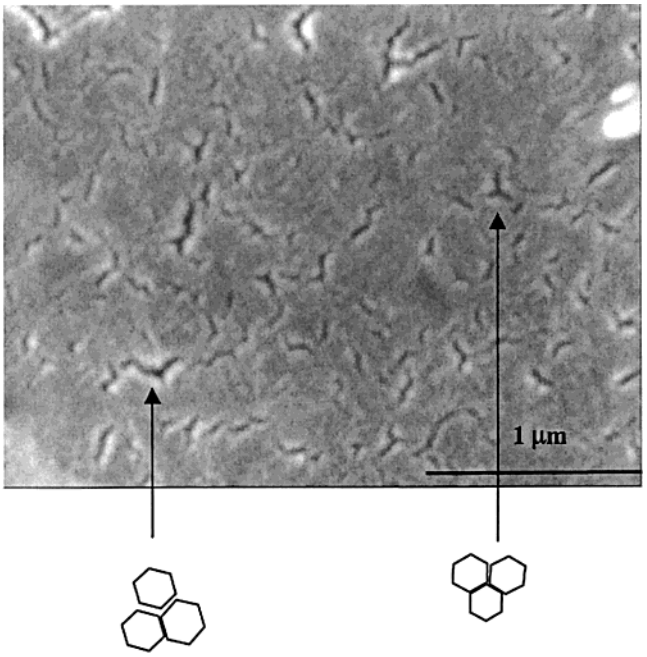

Figure 3. SEM image of the cross section of a film prepared from monomodal LgSf particles. Voids have sizes and shapes that are consistent with particle coalescence in an hexagonal array of 300 nm particles, as illustrated schematically. The bar indicates 1 μm.

The *bulk* morphology of the same type of film was determined by SEM analysis of the film cross-section (Figure 3). Although the film was 4 days old when analyzed, one can clearly see elongated void regions having a length that is of the same order of magnitude as the particle size (300 nm) throughout the bulk of the film. The size of the voids suggests that they result from defects in the particle packing. Particle identity, however, is lost because of particle coalescence, in contrast to what was seen in freshly cast films using AFM.

The requirement of phase continuity, as already described, predicts that the critical volume concentration of the small particles to achieve a continuous network (for the size ratio of 6:1) is ca. 18 wt %. (As the density of the large and small particles are virtually the same, concentrations by weight and volume are equivalent.) AFM analysis of a blend near the V_c (83.5 wt % LgSf and 16.5 wt % SmSf), shown in Figure 4, reveals that, at the film surface, the large particles are completely surrounded by small ones. The latter form a continuous network, which prevents contact between the large particles. Quantitative AFM analysis performed on numerous images indicates that the average center-to-center distance between the large particles is 401 ± 24 nm. Thus, the large particles are not in contact

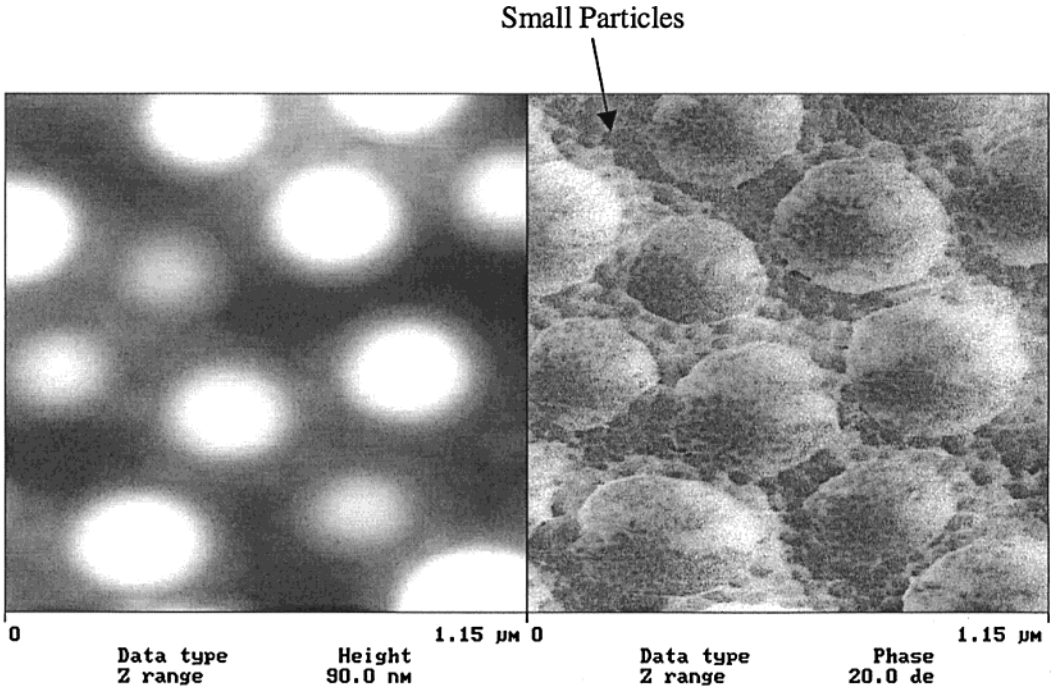

Figure 4. AFMimage of the polymer−air interface of a film prepared from a blend of 83.5 wt % LgSf and 16.5 wt % SmSf particles. The area of the scan is 1.15 μm × 1.15 μm^2. The small particles form a continuous network around the large particles.

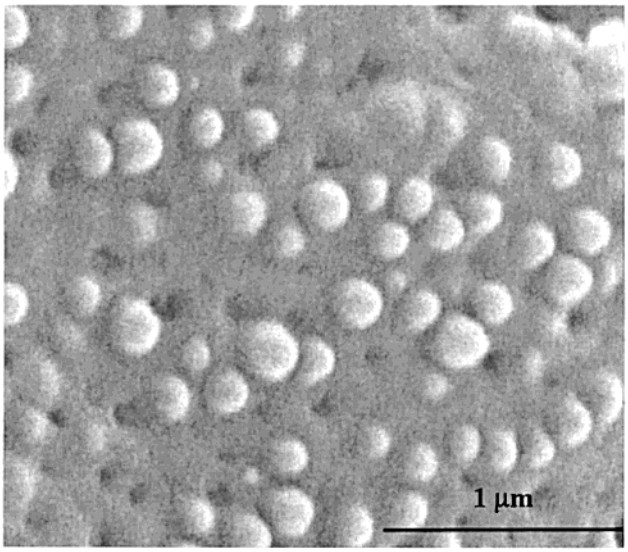

Figure 5. SEM image of the cross section of a blend film having the same composition as in Figure 4 (83.5 wt % LgSf and 16.5 wt % SmSf). The bar represents 1 μm. The large particles are not in an ordered array as at the air surface, but they are nevertheless surrounded by a continuous matrix. The "dimples" are thought to be caused by the pullout of large particles during the fracture process.

with each other below the surface, but are separated by a distance of about 100 nm, which is equivalent to the distance of two small particle diameters. This particle arrangement is consistent with the expectations of models of phase continuity for a concentration of small particles at approximately the critical volume.

To gain further insight into bulk morphology, a cross section of this blend film was analyzed by SEM. Several images were acquired across the bulk of the film (from the polymer/air to the polymer/substrate interface), and no significant variation was observed. In the representative image shown in Figure 5, the morphology in the bulk appears to be very similar to that of the surface. The large particles are well-separated in a continuous network formed by the small particles. Contact between the large particles is seen only on rare occasions. The large particles retain their spherical shape in the bulk as they do at the surface.

Surprisingly, the surface structure of a film prepared from a blend of 90 wt % LgSf and 10 wt % SmSf (Figure 6) appears similar to that of the monomodal LgSf (Figure 4). The surface is dominated by large particles, and there is no evidence for small particles at the polymer/air interface. It would be expected that some small particles would appear at the polymer/air interface, considering that the number ratio of small:large particles is 19:1.

In comparison to the blends of soft particles, Figure 7A shows an AFM image of the polymer/air interface of a film prepared from a blend of 55 wt % LgHd and 45 wt % SmSf particles. The LgHd particles tend to cluster together, as has been also reported elsewhere.[9,16] In some cases, the SmSf particles appear to cover the LgHd particle clusters and bury them below the surface. Because of LgHd particle clustering the film surface is significantly rougher compared to the other blends shown. In some regions, the hard particles create crevices or nanosize cracks at the surface, as if a precursor to the nonfilm formation found at higher concentrations of hard particles. For comparison, Figure 7b shows the surface of a LgSf/SmSf containing approximately the same concentration of large particles. This surface is smoother. The large particles appear for the most part in isolation rather than in clusters. We will discuss later how the optical transparency of the hard/soft blend is reduced in comparison to the soft/soft blend.

In summary of the microscopy analysis, the disordered packing of only partly deformed LgSf particles leads to both high surface roughness and relatively high interparticle void volume concentration. The addition of 16.5 wt % small particles leads to improved particle packing, which is responsible for the reduction of the

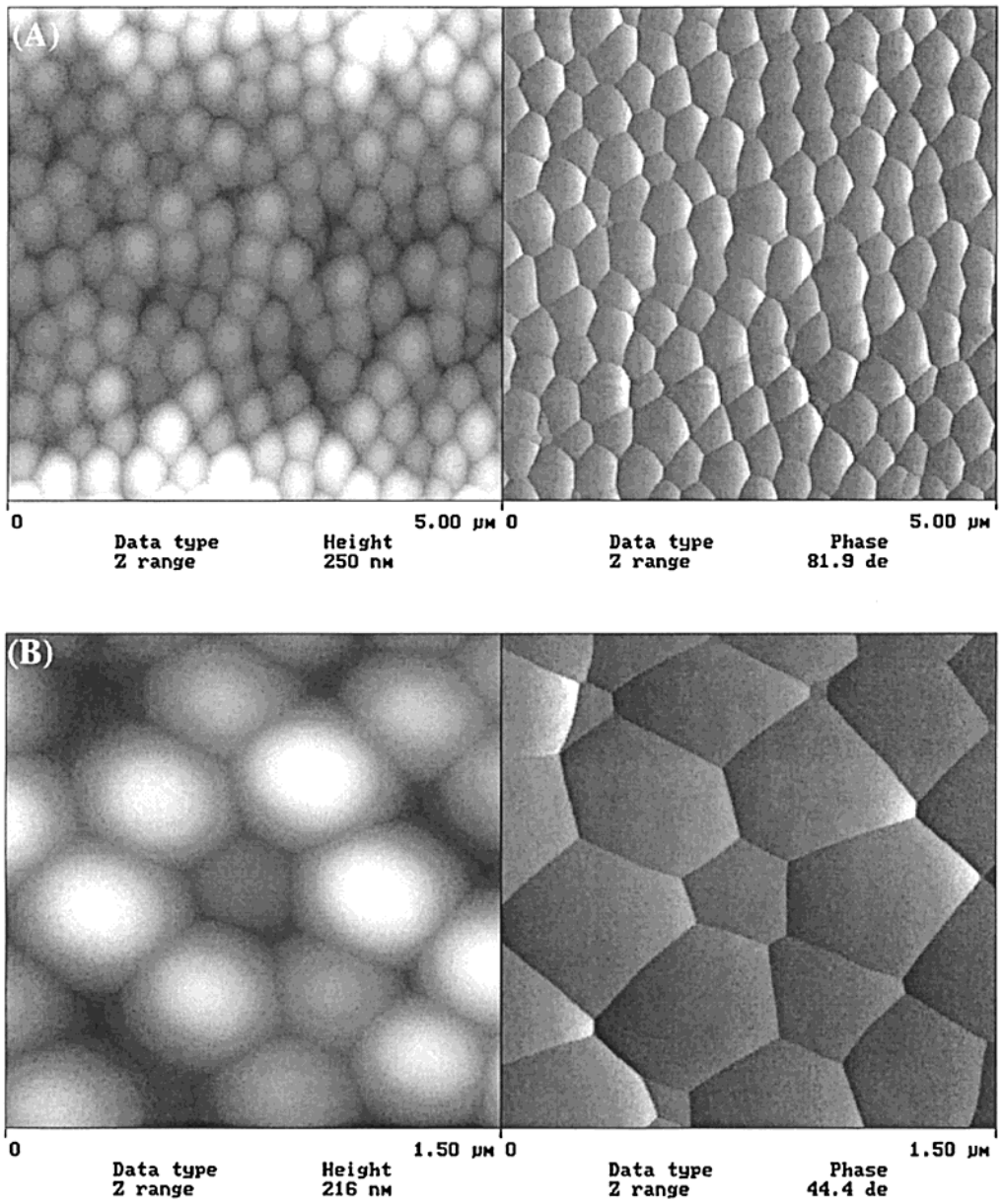

Figure 6. AFM images of the polymer/air surface, prepared from a 90 wt % large latex dispersion. No small particles are apparent at the surface. Key: (A) 5 μm × 5 μm and (B) 1.5 μm × 1.5 μm.

void volume concentration in the bulk. In blends containing large, hard particles, significant void content develops within clusters of the hard particles. (In other AFM and ellipsometry analysis, we have found that the average void size decreases over time as particle deformation continues.)

3.2. Ellipsometry after Film Formation: Void Content and Surface Roughness. Analysis of ellipsometry data requires fitting to a proper theoretical model. Observations of film morphology, reported in section 3.1, can be used to construct such a model. First, we note that the film surfaces are not smooth but have a surface roughness that results from the contours of the individual particles. Second, we note that the bulk of the film contains interparticle voids. We have therefore constructed a model for ellipsometry analysis that consists of a rough layer on top of a bulk layer containing voids, as shown schematically in Figure 8. Both layers are composed of a mixture of dense acrylic polymer and air voids. If the size of the voids is below the wavelength of light, then the refractive index of a layer depends on the volume fraction of voids, as predicted in an effective medium approximation (EMA).[21] Given that n_p is the refractive index of the fully dense polymer at a certain wavelength (measured independently) and that n_v is the refractive index of air voids ($n_v = 1.00$), one can calculate the void concentration from a measurement of the index, n, of a composite film consisting of polymer and voids. According to an EMA model, the volume fraction of voids, f_v, is

$$f_v = \frac{n^2 - n_p^2}{n^2 + 2n_p^2} \frac{n_v^2 + 2n_p^2}{n_v^2 - n_p^2} \tag{4}$$

A rough layer is modeled as consisting of 50 vol % polymer and 50 vol % void. For patterned silicon surfaces, roughness measured with ellipsometry was found elsewhere to equal 1.5 times the root-mean-squared values obtained with AFM.[22] In our experiments, the correlation is in the range 1.5−2.0 and shows some variation. The variations are believed to result

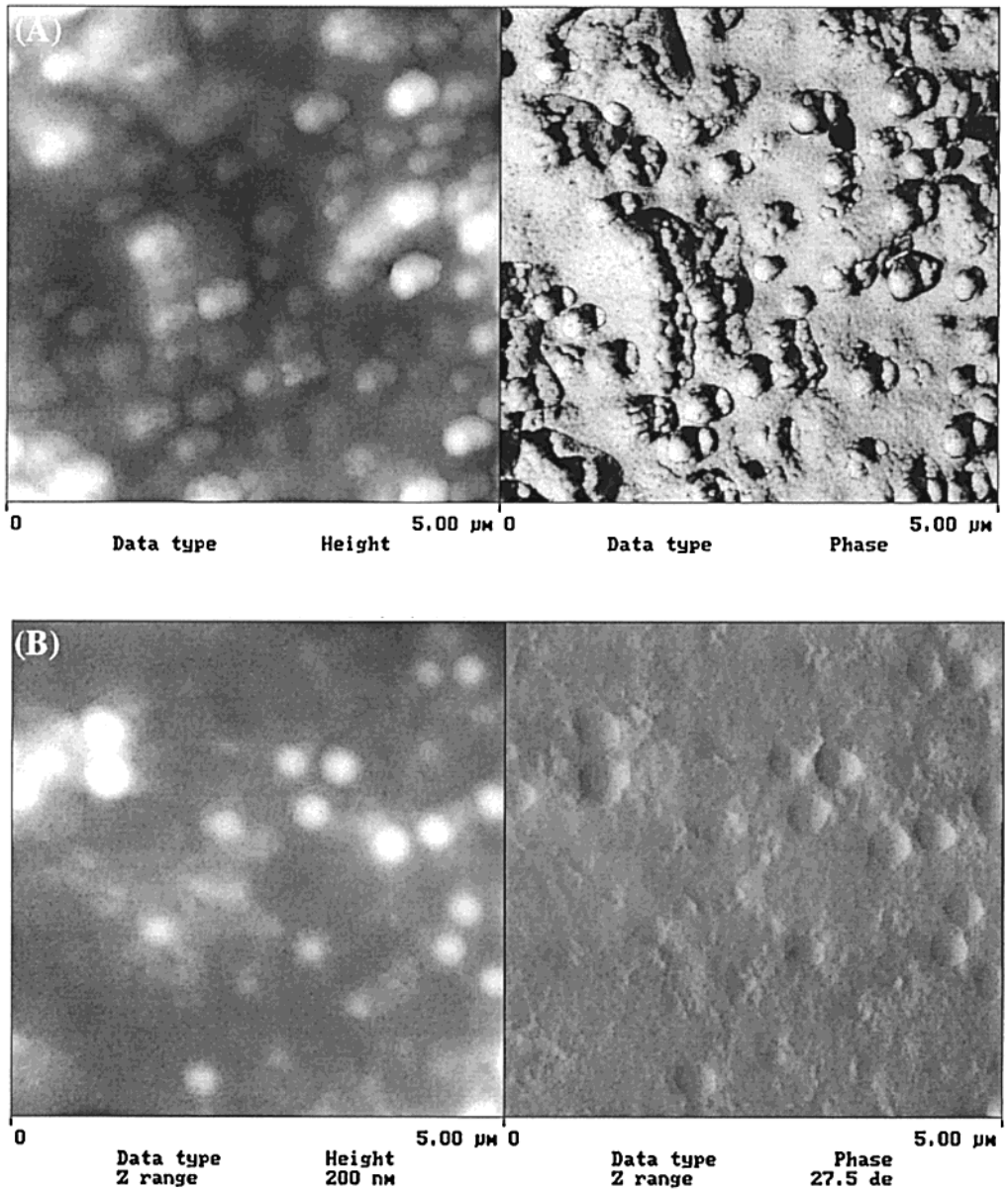

Figure 7. AFM images of the polymer/air interface of a film prepared from (A) a 55 wt % LgHd and 45 wt % SmSf blend and (B) a 56 wt % LgSf and 44 wt % SmSf blend. The image area in both scans are 5 μm × 5 μm. Clustering of LgHd particles is apparent.

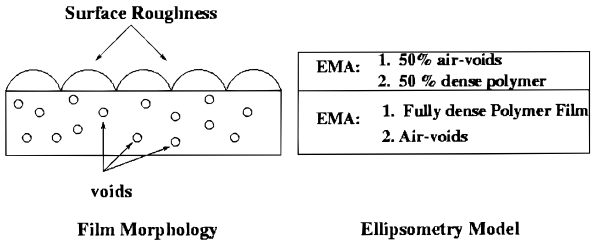

Figure 8. (left) Pictorial illustration of film morphology, in which there is a rough surface caused by particle contours and nanosized air voids distributed in the bulk. (right) Model used to fit and interpret the experimental data acquired by variable-angle ellipsometry. The surface is described as an EMA model with 50% voids and 50% dense polymer material. We fit for the effective thickness of the top layer, which corresponds to surface roughness. The bulk is described with an EMA model for a continuous, dense polymer phase ($n \approx 1.5$) containing voids with $n = 1$. We fit for the volume concentration of voids.

mainly from the different scan sizes analyzed by the two techniques. Ellipsometry analyses a much larger area, which depends on the light beam size and the angle of incidence and is typically 2 mm × 5 mm. AFM scans in this work were over a maximum area of 10 μm × 10 μm. The tip quality also affects the AFM roughness measurements.[23]

Figure 9 shows data obtained in an angular scan of a blend film of soft particles (83.5 wt % LgSf and 16.5 wt % SmSf) obtained 50 min after film casting. The best fit to the data, shown with a solid line, corresponds to a surface roughness of 251 ± 10 nm and a void content of 6.8 ± 0.5 vol %. If we perform a data simulation using a value of 0 for the void fraction, then, as also seen in Figure 9, the theoretical prediction is based on a high refractive index for the film, and the fit is shifted to the right (i.e., to higher angles-of-incidence). If, on the other hand, the surface roughness value in the simulation is changed to 50 nm, then the simulated data has a sharper step in Δ and a lower minimum in Ψ. Thus, it is apparent that the analysis is robust because the two fitting parameters (surface roughness and void concentration) are not strongly correlated. They each can be

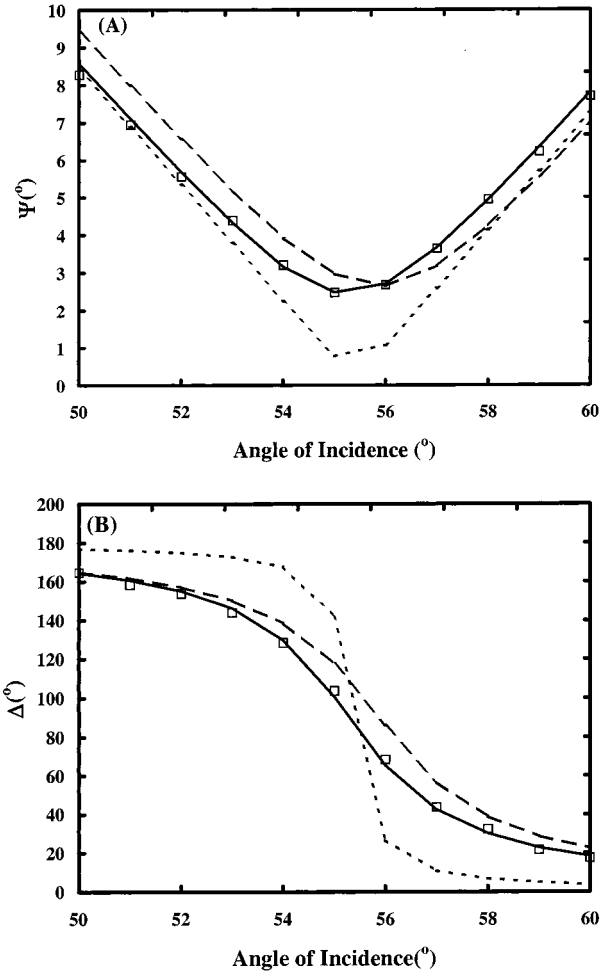

Figure 9. Ellipsometry parameters, Ψ and Δ, obtained from an angular scan obtained from a blend film of 83.5 wt % LgSf and 16.5 wt % SmSf particles using a wavelength of 500 nm. The data were acquired 50 min after casting. The predictions of a model based on a surface roughness of 251 nm and void volume fraction of 6.8 vol % are shown by the solid line. There is good agreement with the experimental data points (—). The simulations for a film with 0% void fraction (– –) but a roughness of 251 nm differ markedly from the best fit. Likewise, the simulations for a film with 50 nm roughness (- - -) deviate from the best fit but in a distinctly different way.

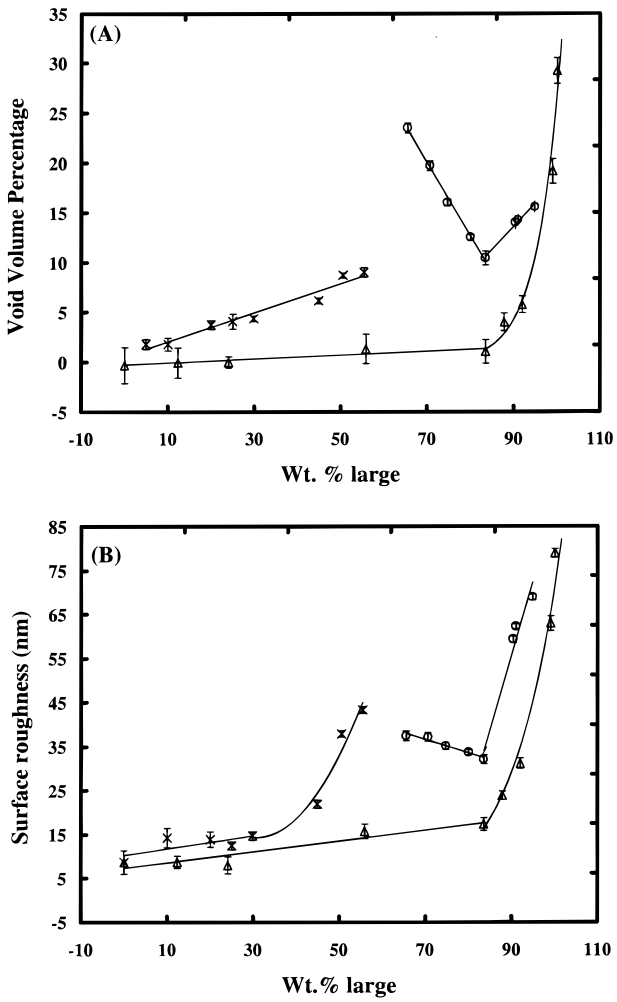

Figure 10. Dependence of the surface roughness and void volume concentration on weight percentage of large particles in bimodal blend films, as determined by ellipsometry. The solid lines are a guide to the eye. The symbols designate films from series 1(LgSf and SmSf) (△), series 2 (LgSf and SmHd) (○), and series 3 (LgHd and SmSf) (×).

independently determined with certainty via the fitting procedure.

The soft and hard particles have slightly different compositions and therefore have slightly different refractive indices, as shown in Table 1. Note that in the mixtures in which the large and small particles have the same composition, the refractive index values of a fully dense film are the same regardless of the relative concentrations. In this case, ellipsometry is therefore insensitive to the *number* ratio of large and small particles per se, although it is highly sensitive to any variation in void content or surface morphology induced by changing this ratio. On the other hand, when analyzing blends of hard and soft particles, the refractive index of the fully dense film can be calculated using an EMA model to be intermediate between the two polymers. This fact is taken into account in the analysis of blend films.

Figure 10 shows the results of ellipsometry analysis of bimodal blends of large and small particles, containing varying fractions of large particles. For consistency and ease of comparison, all measurements were made 1 h after latex casting. Surface roughness and void concentration, obtained by fitting data to the model (Figure 8), are plotted for each series.

When large and small soft particles (T_g = 20 °C) are blended (series 1), then both roughness and void concentration are weakly dependent on the amount of large particles up to a concentration of 83.5 wt % large latex. Above this concentration, there is a marked increase in the measured values of both parameters with increasing concentration of large particles. At least 16.5 wt % small particles are required to obtain a minimization of the void volume concentration. At lower concentrations of small particles, there are insufficient numbers to form a continuous phase around the large particles, and so voids develop. At higher concentrations of small particles, roughness and voids do not change significantly, which is consistent with large particles being isolated in a continuous medium of small particles. The data are thus consistent with the ideas of phase continuity introduced earlier.

We have independently measured the surface roughness of films using AFM analysis. There is a general correlation between the two sets of values. AFM analysis, however, is much more time-consuming, and the film is subject to aging effects during the course of a

measurement. Ellipsometry measurements, in contrast, can be performed within a few minutes. The LgSf particles do not deform fully upon film formation, as observed previously with AFM. Ellipsometry finds there is a surprisingly high fraction of voids in monomodal LgSf films (28 vol %). In a random-close packing of monomodal hard spheres, the void fraction is expected to be in the region of 37 vol %.[5] In a more ordered packing, voids are introduced when particles are missing from the array (i.e., vacancies). In light of these two facts, the experimental value is not implausible when there are partially ordered, partially deformed particles composing the film.

We next consider the results for blends of LgSf and SmHd particles (series 2), also shown in Figure 10. As with the blends of soft particles already discussed, both the void fraction and surface roughness decrease as the concentration of small particles increases from zero until reaching a minimum value at a concentration of 16.5 wt % SmHd (i.e., 83.5 wt % LgSf). At lower concentrations of large particles, there is a greater proportion of nonfilming particles, and this is reflected in a higher void content and a slightly higher surface roughness. Below ~55 wt % LgSf particles, the continuous phase of SmHd particles will not allow film formation. A comparison of series 1 and 2 provides further insight. Near V_c (corresponding to 83.5 wt % large particles) for both series, optimum packing is indicated by the low values of void content. When the small particles are film-forming (series 1), increasing the number of small particles above V_c has little effect. But when the small particles are nonfilm-forming (series 2), the addition of small particles—beyond the number required to create a continuous phase in the void space between large particles—leads to a higher void fraction.

Finally, we consider series 3 (a blend of LgHd and SmSf particles). Previously, Eckersley and Helmer[3] have pointed out that this type of blend is a poor film-former, and our results are consistent with that finding. Figure 10 shows an increase of both roughness and voids upon the addition of LgHd particles. Above 55 wt % LgHd particles, film formation does not occur. In principle, one might expect film formation to be possible as long as there are sufficient numbers of SmSf particles to serve as a "glue" to hold the LgHd particles together. Film formation with up to about 80 wt % large particles would then be possible with this size ratio. However, our AFM analysis (Figure 7) showed that clustering between LgHd particles was unavoidable. Other work[9] has shown that clusters of hard particles create interparticle voids that are filled extremely slowly (i.e., over days) by a soft polymer matrix. Increasing the concentration of LgHd particles thereby increases the void concentration as determined by ellipsometry. The LgHd particles, also apparent in AFM images at the polymer/air interface, are expected to cause an increase in surface roughness. The roughness data from ellipsometry (Figure 10b) suggest that significant numbers of large particles do not appear at the surface below a concentration of ca. 30 wt %.

3.3. Optical Transmission. Ellipsometry analysis is sensitive to the nanovoid volume concentration of a film via its refractive index. Optical transmission measurements, by contrast, are a way of probing the number and size of air voids in a polymer film.[24] Previous workers[25,26] have used Rayleigh scattering theory to relate optical transmission, T, to volume fraction of voids, f_v, via the relationship

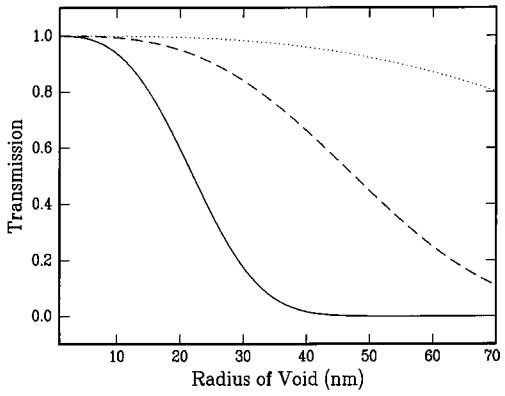

Figure 11. Predicted optical transmission of 100 μm thick films of a continuous medium with $n = 1.5$ and containing spherical air voids ($n_v = 1.0$). The volume fraction of voids (f_v) is taken to be 0.25 (—); 0.025 (— —) and 0.0025 (- - -).

$$\ln T = \left(\frac{-32\pi^4 r_v^3 f_v d}{\lambda^4}\left(\frac{m^2-1}{m^2+2}\right)^2\right) \tag{5}$$

where r_v is the radius of the voids (assuming that they are spherical in shape), d is the optical path length (i.e., film thickness), λ is the wavelength of light, and m is the relative refractive index equal to n_v/n_p, with n_V being the refractive index of air voids ($n_V = 1$) and n_p the refractive index of the fully dense polymer ($n_p = 1.489$ at 500 nm). Note that the number of voids per unit volume, N, is related to f_v

$$N = \frac{3f_v}{4\pi r_v^3} \tag{6}$$

so that transmission measurements can, in principle, be used to determine N provided that other parameters are known. Equation 5 applies only for certain ranges of void size and refractive index. We have tested its applicability by measuring T over a wide range of λ and have found that the dependence of $\ln(T)$ is somewhat weaker than $-\lambda^{-4}$ predicted by eq 5. Nevertheless, optical transmissivity can be qualitatively[24] related to void size and concentration for these films.

Here we use transmission measurements to construct a phase diagram that relates void content to the fraction of large particles, just as elsewhere[2,10,16] transmission measurements have been used to construct phase diagrams for blend films. Figure 11 shows the optical transmission predicted by eq 5, assuming a constant volume fraction of voids with increasing radius. Regardless of the void fraction, transmission decreases with increasing void radius. This figure also demonstrates that, for a void radius of 30 nm, the film can be nearly transparent, nearly opaque, or partially transparent, depending on the void volume fraction (and hence the number of voids per unit volume). In Figure 12 we plot the transmission of films prepared from blends from series 1, 2, and 3. All the films produced from blends of soft particles (series 1) are optically transparent. At the highest concentrations of large particles (above 80 wt % large), there is a slight drop in the transmission. Drawing upon the ellipsometry results, we can conclude that although the void concentration is high, high transparency is achieved from the void size being small.

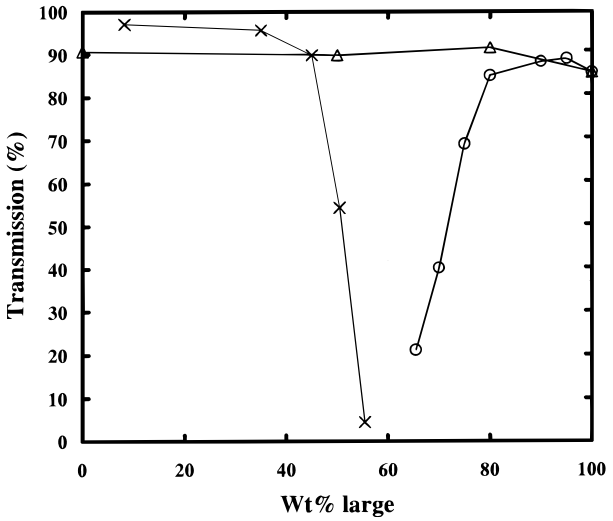

Figure 12. Optical transmission of bimodal blend films from series 1 (△), 2 (○), and 3 (×) as a function of the concentration (weight percent) of large particles. The symbols are the same as used in Figure 10.

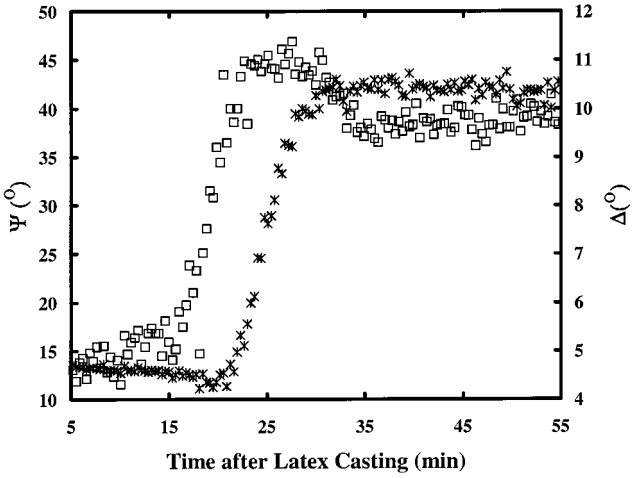

Figure 13. Typical dynamic ellipsometry scan of a film prepared from a latex dispersion of soft particles with a diameter of 300 nm (LgSf). The ellipsometry parameters, Ψ (×) and Δ (□), are plotted vs time after latex casting and while film formation proceeds. Data were obtained using a wavelength of 500 nm was and ϕ_o of 56°.

On the other hand, films prepared from series 2 (LgSf and SmHd) have high transmission only at higher concentrations of large particles. As the SmHd phase is increased, the transmission decreases gradually, which is consistent with more and/or larger voids being present. Ellipsometry indicates an increasing void fraction with an increase of the SmHd phase. The two measurements are thus consistent with each other.

Samples from blends of series 3 (LgHd and SmSf) have high transmission for lower concentrations of the hard particles, which correlates with the low void fractions measured with ellipsometry. As more LgHd particles are added to the dispersion, the transmission of the film is reduced. The void fractions measured with ellipsometry for this series, however, are relatively low. We suggest that the voids probably result from clusters of hard particles and are relatively large in size. They therefore scatter light significantly, so that the optical transmission is reduced. But the overall fraction of voids in the film is low because the relatively small number fraction of LgHd particles are surrounded by a continuous, void-free phase of SmSf particles. This interpretation of the optical data was formulated from observations of film morphology shown in section 3.1.

3.4. Dynamic Ellipsometry Analysis. Until this point, we have described analysis of films *after* their formation. We have also used dynamic ellipsometry scans to probe the morphological changes *during* film formation for blends in each of the series. Figure 13 shows the raw ellipsometry data from a typical dynamic scan obtained during the film formation of a sample prepared from a monomodal LgSf latex dispersion. The two ellipsometric parameters, Ψ and Δ, are plotted as a function of time (where time zero corresponds to casting the wet latex on the substrate). Both Ψ and Δ change substantially within approximately the first 30 min and then evolve at a much slower rate. The region over which the parameters change most abruptly corresponds to the onset of optical clarity, which is usually interpreted as marking the point of film formation. At earlier times, water is the continuous phase in the latex. At later times, there is a continuous polymer layer.

The raw ellipsometry data shown in Figure 13 can be inverted to obtain the complex pseudo-refractive index, $\langle N \rangle$, as a function of time, as shown in Figure 14. Note that $\langle N \rangle = \langle n \rangle + i\langle k \rangle$, where $\langle n \rangle$ is the real component of the pseudo-refractive index and $\langle k \rangle$ is the pseudo-extinction coefficient. The pseudo-refractive index is obtained directly from the ellipticity, ρ (a complex number)

$$\langle N \rangle = \langle N_o \rangle \tan \phi_o \left[1 - \frac{4\rho}{(1+\rho)^2} \sin \phi_o^2 \right]^{1/2} \qquad (7)$$

where $\langle N_o \rangle$ is the complex pseudo-refractive index of the ambient medium, which in our case is air with $\langle N_o \rangle = \langle n_o \rangle = 1$. $\langle N \rangle$ corresponds to the refractive index of the semiinfinite medium leading to the measured ellipticity. Since in the case of latex films, the index is expected to vary in the direction normal to the surface, the pseudo index can be considered to be an *effective* value that is a function of void content, composition and surface roughness. The real component of the pseudo-refractive index, $\langle n \rangle$, will increase with increasing film density and with decreasing void size, both resulting from particle coalescence. A large imaginary component, $\langle k \rangle$, usually indicates a rough surface[27] and will therefore decrease as the film becomes smoother. The value of $\langle k \rangle$ in a dense, optically clear film with a smooth surface is 0. Thus, the pseudo-refractive index of a latex provides qualitative information on the evolution of surface roughness and air voids as influenced by particle deformation during the process of film formation.

Figure 14 compares the $\langle n \rangle$ and $\langle k \rangle$ development of the monomodal LgSf latex to a blend with the addition of only 1 wt % SmSf particles. In both, $\langle n \rangle$ starts off at the value of the refractive index of water (1.33), as would be expected since water is the primary phase at the surface during the early stages of film formation. As water evaporates, particles become more concentrated, causing an increase in the film density that is reflected by the increase of $\langle n \rangle$. After about 20 min, drying nears completion, and the film becomes optically clear. In both the monomodal latex and the blend, $\langle n \rangle$ decreases as $\langle k \rangle$ increases. Our previous microscopy has indicated that freshly formed films do not consist of fully coalesced particles but have significant interparticle voids. The decrease in $\langle n \rangle$ is consistent with the replacement of

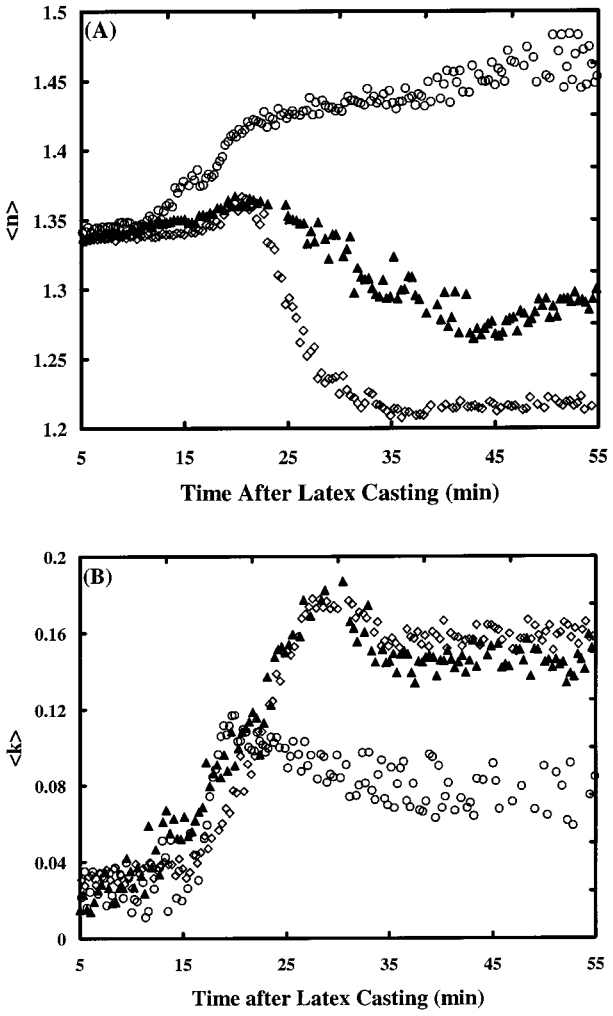

Figure 14. (A) Pseudo-refractive index ($\langle n \rangle$) and (B) the pseudo-extinction coefficient ($\langle k \rangle$) as a function of time after latex casting for three different films. One set of data (shown by ◊) was obtained from the raw data shown in Figure 13 for LgSf particles. Data obtained from the same particles film-formed at 60 °C are shown for comparison (○). Date obtained from a bimodal blend of 99 wt % LgSf and 1 wt % SmSf particles (▲) are also plotted. All experiments were performed with a wavelength of 500 nm and ϕ_o of 56°.

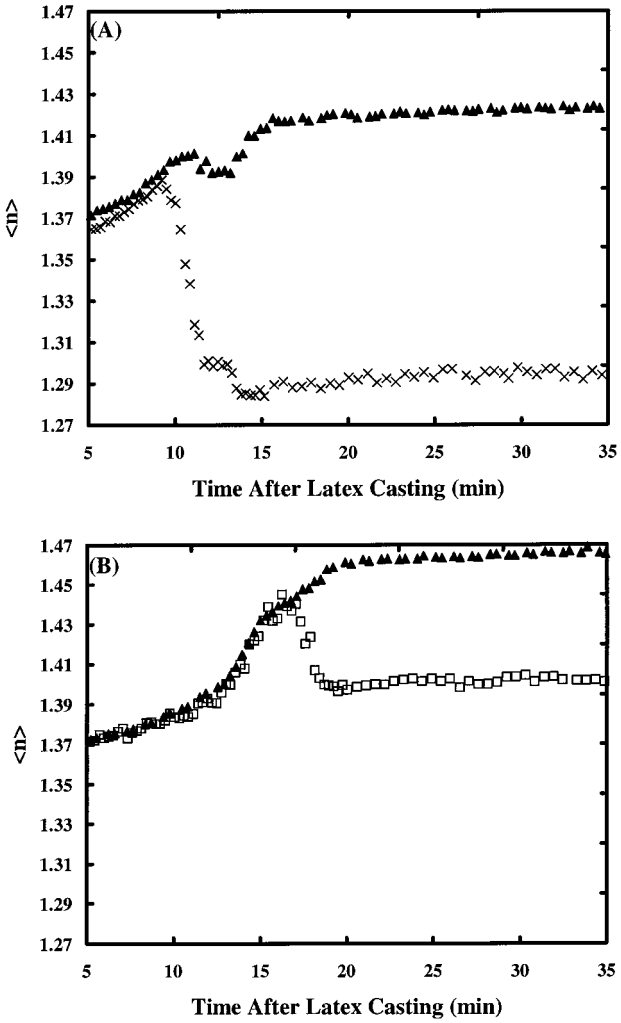

Figure 15. $\langle n \rangle$ during the film formation of bimodal blends. Plots in (A) show data from a blend of 92.0 wt % LgSf and 8.0 wt % SmSf particles (series 1) (▲) in comparison to 90.3 wt % LgSf and 9.7 wt % SmHd particles (series 2) (×). Plots in (B) show data from blends of 83.5 wt % large and 16.5 wt % small particles in series 1 (▲) and series 2 (□). The same axes and symbols are used for parts A and B for ease of comparison.

water—initially present in the interparticle space − by air voids. Since $\langle n \rangle$ is a combination of the refractive index of the polymer ($n = 1.489$ at $\lambda = 500$ nm) and air ($n = 1$), an increase of air voids causes a reduction in $\langle n \rangle$. The decrease of $\langle n \rangle$ corresponds to the lateral passage of the *drying front* in the film. The minimum in $\langle n \rangle$ is attributed to the completion of water evaporation. Thereafter, the particles are expected to eliminate the voids, provided that the particles are deformable. Coalescence of particles is indicated by a very gradual increase of $\langle n \rangle$ over several hours (*coalescence front*). $\langle n \rangle$ of a film prepared from LgHd particles, measured by ellipsometry immediately after the water is evaporated, is ∼1.2. After this film is aged at room temperature for 4 days, $\langle n \rangle$ increases to 1.41, which can be explained by a decrease in void content caused by particle coalescence. With further aging of the film, the refractive index is expected to eventually reach its maximum value (1.489 at 500 nm), when all the voids are eliminated and the film is fully dense.

With the addition of just 1 wt % small particles, Figure 14 shows that $\langle n \rangle$ decreases less upon film formation and $\langle k \rangle$ increases less. This finding is consistent with fewer interparticle voids and a smoother surface caused by small particles packing around the large ones.

As a means of testing our interpretation of the data from dynamic scans, we compare the results from film formation of monomodal LgSf particles at room temperature to what is obtained at a temperature of 60 °C (40 °C higher than the minimum film formation temperature). At the elevated temperature, void coalescence is expected to proceed at an enhanced rate. Figure 14 shows that, in this case, $\langle n \rangle$ increases throughout film formation. This steady increase provides evidence that there is not significant void formation accompanying water loss. After 55 min, the index is close to the value of the fully dense polymer (1.489 at 500 nm), indicating that particle coalescence is nearly complete.

Figure 15 illustrates the effects of substituting SmHd for SmSf particles in bimodal blends containing approximately 91 wt % large particles (Figure 15A) and 83.5 wt % large particles (Figure 15B). The same vertical axes are used in these two plots for ease of comparison. In the blends of series 1 (LgSf and SmSf), there

is a general upward trend in ⟨*n*⟩ during film formation. With 8 wt % SmSf particles, there is a slight decrease in ⟨*n*⟩ at the onset of film formation, which can be interpreted as a result of air void formation. Quickly, however, ⟨*n*⟩ increases again, probably as particle coalescence proceeds and voids diminish. With 16.5 wt % SmSf particles, in comparison, there is no evidence for a separate drying and coalescence front. Instead, ⟨*n*⟩ increases throughout the process and it quickly attains a value of ∼1.47, which is close to what is expected for a fully dense film. This more efficient film formation is consistent with the measurements of void concentration presented previously in Figure 10. This finding complements the weight loss measurements performed by Peters et al.[13] According to their result, at a concentration of 20% SmSf, there is a continuous and linear increase of the drying rate with increasing solids percentage. They suggested that there is therefore a single drying mechanism for this blend, just as we find that there is a continuous change in optical constants. In monomodal systems and other blends, on the other hand, the drying rate changes after a certain solids concentration. The authors considered Croll's model of drying[28] and interpreted the change in the drying rate as a result of the transition layer (with small amounts of water in a porous structure) reaching the substrate. In the present work, we find evidence for voids at the surface, as expected in the Croll model.

In the blends of series 2 (LgSf and SmHd), the efficiency of film formation, as indicated in Figure 15, is not as high. With both 9.7 wt % and 16.5 wt % small, hard particles, a significant drop in ⟨*n*⟩ suggests the formation of air voids with the drying of water. With a greater concentration of small particles (near V_c where the small particles form a continuous phase), the index drop is lower, which probably is because there is a lower concentration of voids. It should be noted that the scans of series 1 and series 2 blends differ dramatically, but their differences cannot be attributed to differences in either particle size or in concentration. The only difference between the two series is the relative hardness of the small particles.

Figure 16 likewise compares the film formation of two different series. Bimodal blends containing approximately 50 wt % large particles are compared: one composed of LgSf and SmSf particles (series 1) and the other composed of LgHd and SmSf particles (series 3). A scan obtained from monomodal SmSf particles is shown for comparison. As expected, the monomodal soft particles form films with maximum density almost immediately upon water evaporation, as indicated by the sharp rise in ⟨*n*⟩ to about 1.49. With the addition of 50 wt % LgSf particles, AFM analysis reveals a matrix of coalesced small particles surrounding isolated large particles. Figure 16 shows that the behavior of this blend is nearly identical to the monomodal latex. The small particles apparently dominate the film formation characteristics by making a dense continuous phase, and LgSf particles do not interrupt it. In contrast, a similar concentration of hard particles has a substantial impact on the film formation. There is a marked drop in ⟨*n*⟩ at the onset of film formation, which can be explained by voids being formed within clusters of LgHd particles, as observed with AFM.

4. Further Discussion

The dynamic ellipsometry analysis of films prepared from bimodal blends of soft particles during the early

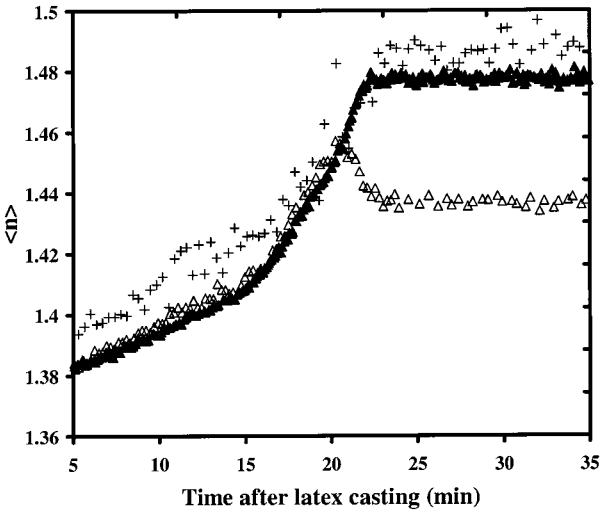

Figure 16. ⟨*n*⟩ during the film formation of bimodal blends and a monomodal small latex dispersion. Plots show data from a blend of 56.0 wt % LgSf and 44 wt % SmSf particles (series 1) (▲) in comparison to a blend of 50.0 wt % LgHd and 50.0 wt % SmSf particles (series 3) (△). Data from a monomodal latex of 50 nm soft particles (SmSf) is shown for comparison (+).

stages of film formation reveals significant differences as the concentration of small particles is varied. Comparison of the data in Figures 14, 15, and 16 allows one to see the trend in series 1 blends with increasing concentrations of LgSf particles. When the concentration of small particles is *above* V_c, such as in the 56 wt % LgSf/44 wt % SmSf blend (Figure 16), there is a sharp and steady increase in ⟨*n*⟩ near the end of the drying period. At the end of drying, a plateau value of ⟨*n*⟩, corresponding to the value of a dense film, is obtained. At concentrations of SmSf particles *below* V_c, e.g., 8 wt % (Figure 15A), 1 wt %, and 0 wt % (Figure 14), there is a clear drop in ⟨*n*⟩ upon completion of drying, possibly indicative of the formation of air voids with water loss. This drop is followed by an increase in ⟨*n*⟩ over time, which results from the decrease in void concentration caused by particle coalescence. This so-called coalescence front is most obvious in the 92 wt % LgSf/8 wt % SmSf blend in which the drop in ⟨*n*⟩ is small and is followed immediately by a sharp rise. At or above a concentration of 16.5 wt % SmSf particles, which is approximately the value of V_c for this size ratio, ⟨*n*⟩ increases steadily with time and shows no evidence for a separate drying and coalescence front. The high value of ⟨*n*⟩ that shows a very slight increase over time, which is observed in Figure 15B, indicates that, although low in concentration, voids close over time. AFM and SEM analysis of this film morphology reveals efficient film formation, in support of the ellipsometry data. In all cases in which there is evidence for voids, ⟨*n*⟩ and ⟨*k*⟩ change steadily with time. Thus, the initial differences between latex blend films narrow with passing time.

Dynamic analysis of series 2 films (LgSf and SmHd particles) reveals that for all of the samples analyzed, a drying front (defined by a drop in ⟨*n*⟩) is followed by a coalescence front (defined by a gradual rise in ⟨*n*⟩). This result indicates that air voids develop during the drying of particles. The volume fraction of voids is a function of the concentration of small particles. At a concentration of 16.5 wt % SmHd particles, the magnitude of the drop in ⟨*n*⟩, and hence the void content, is minimized. Variable angle ellipsometry provides a reliable, quantitative measurement of both surface roughness and

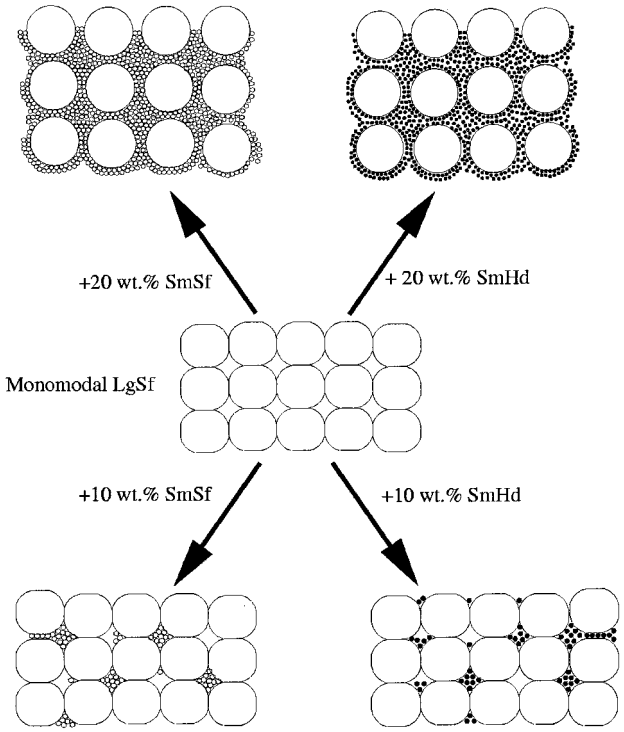

Figure 17. Schematic illustration of various morphologies in bimodal blend films based on LgSf particles (series 1 and 2) above and below V_c for this size ratio. The particle sizes are not drawn to scale.

void content that is consistent with these findings from the dynamic scans.

Our conclusions for films containing LgSf particles (series 1 and 2) are summarized in Figure 17. When the concentration of small particles is at or above V_c, the large particles do not deform from their spherical shape but are separated from each other by small particles. The film formation behavior of the small particles then determines the void content in the film. When the concentration of small particles is below V_c, the interparticle space of the large particles is not completely filled by the small particles. Consequently, with both hard and soft small particles, voids are present in the film, but even more so with the former.

When the small particles are soft, they form a continuous matrix at concentrations above V_c. In contrast, when the small particles are hard, they introduce new voids at concentrations above this value. Thus, with the addition of SmHd particles to LgSf particles, there is a gradual transition from the situation in which voids between the partly deformed, 300 nm particles are dominant to a situation in which a greater number of small voids between 50 nm particles is dominant. With 16.5 wt % SmHd particles, which is near V_c, the voids concentration due to the two types of particles achieves a minimum.

Figure 18 compares the morphologies of series 3 films. Clusters of hard particles create air voids and subsequent film opacity. Clustering of large, hard particles has also been observed elsewhere.[9,16,29] Tang et al.[29] correlated the extent of cluster formation with the concentration of carboxyl groups at poly(styrene) particle surfaces. A higher concentration of carboxyl groups (e.g., 77% coverage) resulted in an increased amount of cluster formation. We saw no evidence for the clustering of LgSf particles, but we are unable to provide an

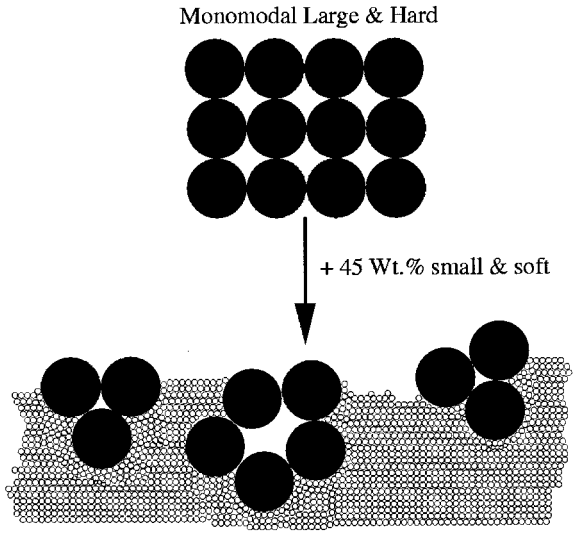

Figure 18. Schematic illustration of the clustering of LgHd particles in a blend with SmSf particles (series 3) leading to the creation of large air voids.

explanation for the differences observed. If LgSf particles were to cluster, however, particle coalescence would cause a gradual decrease in the void size formed, while hard particles create larger, longer-lasting voids.

We recall that a number ratio of large to small particles of 1:1 is required to achieve a colloidal crystal with the sodium chloride or zinc blende structures. With the particle size ratio of 6:1 used here, such a crystal is geometrically feasible, provided that there are about 99 wt % large particles (as required for a 1:1 number ratio according to Table 2). Our ellipsometry analysis of 99 wt % large bimodal blend films reveals a significant fraction of voids, thereby indicating that the optimum packing of a colloidal crystal was unsurprisingly not achieved.

Finally, we consider why ellipsometry indicates significant void content in monomodal LgSf films but much less in SmSf films. The driving force for film formation is proportional to the inverse of the particle size, according to descriptions of film formation driven by capillary forces.[1] The greater curvature and higher surface area of small particles are expected to encourage film formation and thereby lead to films with lower void content. Previous workers[8,30,31] have demonstrated that smaller particles have a lower MFT for these reasons. Moreover, Sperry and co-workers,[31] using a geometric argument, have proposed that it should take a longer time for voids to close in a latex film based on larger particle sizes. In light of these past results and theoretical work,[32] in latex dispersions of larger particles, poorer film formation and a greater void fraction at a given time are expected in comparison to an identical latex with smaller particles. Thus, polymer particles with the same glass transition temperature and presumably the same mechanical properties but with different sizes (i.e., LgSf and SmSf) form films with differing void concentrations. Blends dominated by LgSf particles have a high void fraction, whereas films containing a fraction of SmSf particles greater than V_c have a much lower void fraction, as seen for series 1 in Figure 10. Increasing the SmHd particles of series 2 above about 16.5 wt % (i.e., above V_c), in stark contrast, leads detrimentally to higher void content.

5. Concluding Summary

We have presented evidence that achieving the critical volume fraction of small particles required for continuity in bimodal latex blends can be correlated to the creation of a film with low void content. For the ratio of large:small diameters studied here (ca. 6:1), above a volume fraction of small particles of about 0.18, a theory of continuity predicts that a continuous phase of small particles is formed. At about this same fraction of small particles in bimodal blends of soft particles, we find a transition between films with higher void contents and those with lower void contents. If the small particles are hard (i.e., non-film-forming), the void fraction attains a minimum at V_c. At higher concentrations of SmHd particles, instead of merely filling the void space between the large particles, the small particles create additional voids in the matrix surrounding the large particles. Additionally, films cannot be formed with high weight fractions of large hard particles. At relatively low concentrations (30 wt %), the hard particles form clusters that create air voids and nanocracks. It is therefore not possible to obtain a film consisting of *isolated* large hard particles surrounded by a matrix of film-formed soft particles at the V_c value of ca.18 wt %.

Acknowledgment. A.T. gratefully acknowledges the Engineering and Physical Sciences Research Council and Zeneca Resins for a PhD studentship. The VASE instrument was partly funded by a grant from the EPSRC. We gratefully acknowledge helpful discussions with Drs. J. R. Lu and R. P. Sear (University of Surrey).

References and Notes

(1) Keddie, J. L. *Mater. Sci. Eng. Rep.* **1997**, *R21/3*, 101.
(2) Winnik, M. A.; Feng, J. *J. Coat. Technol.* **1996**, *68*, 39.
(3) Eckersley, S. T.; Helmer, B. J. *J. Coat. Technol.* **1997**, *69*, 97.
(4) Chu, F. X.; Graillat, C.; Guyot, A. *J. Appl. Polym. Sci.* **1998**, *70*, 2667.
(5) Russel, W. B.; Saville, D. A.; Schowalter, W. R. *Colloidal Dispersions*; Cambridge University Press: Cambridge, England, 1989; p 466, p 341.
(6) Ashcroft, N. W.; Mermin, D. *Solid State Physics*; Saunders College: Philadelphia, PA, 1976; p 387.
(7) Bartlett, P.; Ottewill, R. H.; Pusey, P. N. *Phys. Rev. Lett.* **1992**, *68*, 3801.
(8) Geurts, J. M.; Lammers, M.; German, A. L. *Colloids Surf. A: Physicochem. Eng. Aspects* **1996**, *108*, 295.
(9) Keddie, J. L.; Meredith, P.; Jones, R. A. L.; Donald, A. M. *Langmuir* **1996**, *12*, 3793.
(10) Feng, J.; Winnik, M. A.; Shivers, R. R.; Clubb, B. *Macromolecules* **1995**, *28*, 7671.
(11) Dullen, F. A. L. *Porous Media: Fluid Transport and Pore Structure*, 2nd ed.; Academic Press: London, 1992; p 77.
(12) Kusy, R. P. *J. Appl. Phys.* **1977**, *48*, 5301.
(13) Peters, A. C. I. A.; Overbeek, G. C.; Buckmann, A. J. P.; Padget, J. C.; Annable, T. *Prog. Org. Coat.* **1996**, *29*, 183.
(14) Binnig, G.; Quate, C. F.; Gerber, Ch. *Phys. Rev. Lett.* **1986**, *56*, 930.
(15) Hellgren, A.-C. *Prog. Org. Coat.* **1998**, *34*, 91.
(16) Patel, A. A.; Feng, J.; Winnik, M. A.; Vancso, G. J.; Dittman McBain, C. B. *Polymer* **1996**, *37*, 5577.
(17) Snyder, P. G.; Rost, M. C.; Bu-Abbud, G. H.; Woollam, J. A. *J. Appl. Phys.* **1986**, *60*, 3293.
(18) Styrkas, D.; Doran, S. L.; Gilchrist, V.; Keddie, J. L.; Lu, J. R.; Murphy, E.; Sackin, R.; Su, T.-J.; Tzitzinou, A. In *Polymer Surfaces and Interfaces III*; Richards, R. W., Peace, S. K., Eds.; John Wiley & Sons: London, 1999; p 1.
(19) Keddie, J. L.; Meredith, P.; Jones, R. A. L.; Donald, A. M. *Macromolecules* **1995**, *28*, 2673.
(20) Keddie, J. L.; Meredith, P.; Jones, R. A. L.; Donald, A. M. *Film Formation in Waterborne Coatings*; Provder, T., Winnik, M. A., Urban, M. W., Eds.; ACS Symposium Series 648; American Chemical Society, Washington, DC, 1996; p 332.
(21) Aspnes, D. E.; Theeten, J. B.; Hottier, F. *Phys. Rev. B* **1979**, *20*, 3292.
(22) Koh, J.; Lu, Y.; Wronski, C. R.; Kuang, Y.; Collins,R. W. *Appl. Phys. Lett.* **1996**, *69*, 1297.
(23) Fang, S. J.; Chen, W.; Yamanaka, T.; Helms, C. R. *Appl. Phys. Lett.* **1996**, *68*, 2837.
(24) Meeten, G. H. *Optical Properties of Polymers*; Elsevier Applied Science Publishers: London, 1986; p 29.
(25) Van Tent, A.; Te Nijenhuis, K. *Prog. Org. Coat.* **1992**, *20*, 459.
(26) Van Tent, A.; Te Nijenhuis, K. *J. Colloid Interface Sci.* **1992,** *150*, 97.
(27) Urban, F. K., III; Ruzakowski Athey, P.; Islam, Md. S. *Thin Solid Films* **1994**, *253*, 326.
(28) Croll, S. G. *J. Coat. Technol.* **1986**, *58*, 41.
(29) Tang, J. S.; Dimonie, V. L.; Daniels, E. S.; Klein, A.; El-Aasser, M. S.; *Abstracts of Papers, American Chemical Society*; American Chemical Society: Washington, DC, 1999; Vol. 218, Part 2; 61-PMSE.
(30) Jensen, D. P.; Morgan, L. W. *J. Appl. Polym. Sci.* **1991**, *42*, 2845.
(31) Sperry, P. R.; Snyder, B. S.; O'Dowd, M. L.; Lesko, P. M. *Langmuir* **1994**, *10*, 2619.
(32) Routh, A. F.; Russel, W. B. *Langmuir* **1999**, *15*, 7762.

MA991372Z